Modular and Predictable Assembly of Porous Organic Molecular Crystals

James T. A. Jones,[1] Tom Hasell,[1] Xiaofeng Wu,[1] John Bacsa,[1] Kim E. Jelfs,[1] Marc Schmidtmann,[1] Samantha Y. Chong,[1] Dave J. Adams,[1] Abbie Trewin,[1] Florian Schiffman,[2] Furio Cora,[2] Ben Slater,[2] Alexander Steiner,[1] Graeme M. Day[3]* and Andrew I. Cooper[1]*

1 Department of Chemistry and Centre for Materials Discovery, University of Liverpool, Crown Street, Liverpool, L69 7ZD, United Kingdom. E-mail: aicooper@liv.ac.uk
2 Department of Chemistry, University College London, 20 Gordon Street, London, WC1H 0AJ , United Kingdom, E-mail: f.schiffmann@ucl.ac.uk
3 Department of Chemistry, University of Southampton, Highfield, Southamtpon, SO17 1BJ, United Kingdom. E-mail: gmd1a11@soton.ac.uk

Please cite this paper as:

Nature, 2011, *474,* 367–371

The publisher's version of this paper is available here:
http://dx.doi.org/10.1038/nature 10125

Modular and Predictable Assembly of Porous Organic Molecular Crystals

James T. A. Jones,[1] Tom Hasell,[1] Xiaofeng Wu,[1] John Bacsa,[1] Kim E. Jelfs,[1] Marc Schmidtmann,[1] Samantha Y. Chong,[1] Dave J. Adams,[1] Abbie Trewin,[1] Florian Schiffman,[2] Furio Cora,[2] Ben Slater,[2] Alexander Steiner,[1] Graeme M. Day[3*] and Andrew I. Cooper[1*]

[1] Department of Chemistry and Centre for Materials Discovery, University of Liverpool, Crown Street, Liverpool, L69 7ZD, United Kingdom. E-mail: aicooper@liv.ac.uk

[2] Department of Chemistry, University College London, 20 Gordon Street, London, WC1H 0AJ , United Kingdom, E-mail: f.schiffmann@ucl.ac.uk

[3] Department of Chemistry, University of Cambridge, Lensfield Road, Cambridge, CB2 1EW, United Kingdom. E-mail: gmd27@cam.ac.uk

Nanoporous molecular frameworks[1-7] are important in applications such as separation, storage, and catalysis. Empirical rules exist for their assembly but it is still challenging to place and segregate functionality in three-dimensional porous solids in a predictable way. Indeed, recent studies on mixed crystalline frameworks suggest a tendency for statistical distribution of functionalities throughout the pores[7] rather than, for example, the functional group localisation found in the reactive sites of enzymes[8]. This is a potential limitation for 'one-pot' chemical syntheses of porous frameworks from simple starting materials. An alternative strategy is to prepare porous solids from synthetically pre-organised molecular pores[9-15]. In principle, functional organic pore modules could be covalently prefabricated and then assembled to produce materials with specific properties. However, this mix-and-match assembly vision is far from realized, not least because of the challenge in reliably predicting 3-dimensional structures for molecular crystals which lack the strong directional bonding found in networks. We show here that highly-porous crystalline solids can be produced by mixing different organic cage modules which self-assemble via chiral recognition. Importantly, the structures of the resulting materials can be predicted computationally[16-17], allowing *in silico* materials design strategies.[18] The constituent pore modules are synthesized in high yields on gram scales in a one-step reaction. Assembly of the porous cocrystals is as simple as combining the modules in solution and removing the solvent. In some cases, the chiral recognition between modules can be exploited to produce porous organic nanoparticles. The method is not limited to one molecular combination but can be generalised in a computationally predictable manner based on a lock-and-key assembly between modules.

A basic tool in the synthesis of functional extended solids is the ability to combine different chemical entities in a controlled and modular fashion. This has been demonstrated for structurally related or 'isoreticular' porous metal-organic frameworks (MOFs)[3]. MOFs can be prepared with more than one chemical function, either by direct reaction of mixed precursors[7] or by post-synthetic modification[19]. While both MOFs and also zeolites can comprise fused, compartmentalized cages, it is still generally challenging to segregate structural units in a programmed and predictable way. Most nanoporous networks are synthesized in 'one-pot' chemical reactions where all of the precursors are mixed together simultaneously[1-7]. The 3-dimensional network structure arises from self-assembly of the components. By contrast, natural products are synthesized via stepwise reaction sequences where isolable molecular intermediates are elaborated and combined to create more complex structures. An analogous, supramolecular strategy[20] for porous organic solids would be to preorganize larger chemical sub-units, or pore modules, prior to assembling the extended crystal. This approach requires building blocks or tectons[21-22] that are self-assembling, prefabricated molecular analogues of the secondary building units in networks such as MOFs[1-5,7]. To be broadly useful, the pore modules should pack together in predictable ways. Individual modules could then be designed to incorporate desirable chemical functionalities, either by chemical derivatization[15] or by physical encapsulation within the molecular pores[23]. Mixing different functional modules might produce porous solids with unusual properties: perhaps, for example, by combining both acid- and base-containing cage modules within the same porous solid along with vacant, flow-through pores. In practice, however, many components of this strategy are currently missing. While a large number of porous molecular solids are known[9-15], as highlighted in a recent review[24], the rules that underpin their three-dimensional non-covalent assembly are poorly understood. In this respect, Desiraju's vision of 'supramolecular synthesis'[20] is still unfulfilled. Levels of porosity in such molecular organic solids are also modest: until recently[12-15], Brunauer-Emmett-Teller surface areas, SA_{BET}, of less than 400 $m^2\ g^{-1}$ were typical[24]. Moreover, porous molecular solids could not be described as modular because almost all examples are single-component crystals.

In this study, we report the first porous organic molecular cocrystals, thus demonstrating a new modular assembly concept. We also describe computational methods to predict these crystal structures *ab initio*, greatly enhancing the long-term prospects for rational materials design[18]. The materials were fabricated from combinations of the four pore modules shown in

Fig. 1a. The first porous cocrystal was constructed from two organic cages that we described previously[12]: cage **1** and cage **3**-*R*. Porosity is covalently prefabricated in the individual tetrahedral cage molecules such that each module has four triangular pore windows with diameters of around 6 Å (Fig. 1a; see also Scheme 1, Supplementary Information). Each cage is just over 1 nm in size. Both cage modules have helical chirality: **1** comprises, in crystalline form, an equimolar mixture of the helical enantiomers **1**-*S* and **1**-*R*[12,14] while **3**-*R* is homochiral. Both cages are soluble in common solvents and can be simply mixed together in solution. Slow evaporation of an equimolar solution of **1** and **3**-*R* did not lead to separate crystals of the individual modules, but rather to a new single-phase crystalline material. Remarkably, the material is a quasiracemic cocrystal[25], (**1**-*S*, **3**-*R*). That is, it consists exclusively of the *S* helical enantiomer of **1** crystallized with **3**-*R* (Fig. 1b). The apparent loss of the **1**-*R* enantiomer, despite 100 % sample mass recovery from crystallisation, is explained by variable temperature ^{1}H nuclear magnetic resonance measurements. This shows that the helical configuration of **1** interconverts rapidly in solution (Supporting Information, Fig. S2)[14]. The chirality of **1** is therefore dynamically resolved upon crystallisation with the homochiral cage, **3**-*R* (Fig. 2a). Cage **1** is an 'amphichiral' module: it can also pair with **3**-*S* to form the opposite quasiracemic cocrystal, (**1**-*R*, **3**-*S*). As discussed below, however, this assembly strategy is not limited to dynamically chiral molecules.

The crystal packing for (**1**-*S*, **3**-*R*) is also shown in Fig. 2a: the **1**-*S* and **3**-*R* modules alternate in the crystal lattice in a face-centred cubic arrangement, analogous to the ZnS 'zinc blende' structure. Each cage forms window-to-window interactions with four partner cages of the other type. The result is an interconnected diamondoid pore network. No polymorphs of pure **1** have been found which pack in a window-to-window fashion.[12,14] As such, this packing mode is directed by the presence of the chiral co-module, **3**-*R*. The window-to-window packing arrangement creates permanent pore channels in the cocrystal, which displays a type I nitrogen sorption isotherm at 77 K (Fig. 2b) and a surface area, SA_{BET}, of 437 $m^2 g^{-1}$. Like the other materials described here, the cocrystal is stable towards desolvation and has good thermal stability, showing little weight loss until the onset of decomposition at 350 °C (Fig. S7).

The heterochiral (**1**-*S*, **3**-*R*) pairing can be considered as a directional tecton[22], comparable with reversible supramolecular interactions such as hydrogen bonding[21] and the

'sextuple aryl embrace'[26] which involves interlocking aryl rings. Density functional theory (DFT) calculations for isolated cage pairs indicate that the heterochiral window-to-window interaction is 18 kJ mol^{-1} more stable than the equivalent homochiral interaction, and much more stable than other hypothetical window-to-arene or arene-to-arene pairs which would lead to disconnected pores (Fig. S8). Lattice energy calculations confirm that this heterochiral pairing preference carries over to the solid state and, more significantly, that the observed cocrystal structure can be predicted *ab initio* from the molecular formulae of the modules. Calculations employing Monte Carlo simulated annealing to generate hypothetical (**1**-*S*, **3**-*R*) crystal structures, followed by energy minimisation using anisotropic atom-atom potentials[27-28], showed the observed packing mode for (**1**-*S*, **3**-*R*) to be the global lattice energy minimum (Fig. 3), with good agreement between the *ab initio* predicted structure and the experimental single crystal X-ray structure (Fig. 3a). The most stable hypothetical homochiral (**1**-*R*, **3**-*R*) structure, which lacks window-to-window packing, was predicted to be 18.8 kJ mol^{-1} less stable than the observed (**1**-*S*, **3**-*R*) quasiracemate. These calculations therefore rationalise the preference for **1** to adopt the **1**-*S* configuration in the cocrystal and to pack in a window-to-window fashion: that is, both the preferred chirality and the resultant porosity in the solid can be predicted *ab initio*. To verify the atom-atom potential lattice energy calculations, solid state DFT calculations were performed on the observed quasiracemate and low-energy predicted homochiral structures: these calculations confirmed the preference for heterochiral packing.

This behaviour is not limited to the **1**-*S* / **3**-*R* pairing. The enantiomers **3**-*S* and **3**-*R* also strongly prefer heterochiral window-to-window pairs and assemble in that fashion in a (**3**-*S*, **3**-*R*) racemic crystal (Fig. 1c) to give a porous solid with SA_{BET} of 873 m^2 g^{-1}. In this case, the chirality in both modules is fixed rather than dynamic. As before, DFT simulations suggest a significant energy gain (19 kJ mol^{-1}) in the formation of heterochiral dimers. Again, the crystal structure can be predicted *ab initio*. The experimentally-observed racemic packing is the global energy minimum in the set of predicted crystal structures and there is close agreement between the predicted and observed structures (Fig. 3c). These calculations also suggest a global preference for heterochiral rather than homochiral packing modes. A large energetic gain of 32 kJ mol^{-1} is calculated for the (**3**-*S*, **3**-*R*) racemic crystal over the most stable predicted homochiral structure for **3**-*R*. The global minimum homochiral prediction also closely reproduces the observed structure for **3**-*R*[12] (Fig. 3b) which, unlike **1**, can be obtained from

enantiopure solutions because **3**-*R* it does not interconvert with its enantiomer. As for the (**1**-*S*, **3**-*R*) cocrystal, the atom-atom lattice energy calculations were verified using periodic DFT calculations, which resulted in similar calculated energy differences (Table S1, Fig. S13). An analogous set of experimental observations and crystal structure predictions was obtained for a new cage module, **4**-*S*, which has cyclopentane rather than cyclohexane vertices (Fig. 1a). This module forms a quasiracemic cocrystal, (**4**-*S*, **3**-*R*), with SA_{BET} of 980 $m^2 g^{-1}$. In this case, the predicted global energy minimum crystal structure is an ordered version of the most probable site-disordered $F4_132$ structure based on powder X-ray data (Figs. S12, S15). By itself, **4**-*S* does not pack in a window-to-window fashion (Fig. S18). Hence like, (**1**-*S*, **3**-*R*), this packing mode is directed by the partner module, **3**-*R*.

Not all systems favour heterochiral assembly and this, too, is predictable from the calculated crystal energy landscape. A new module, **5**-*R* (Fig. 1a), was synthesized by the [4 + 6] cycloimination reaction between tri(4-formylphenyl)amine and the chiral diamine, (*R*,*R*)-1,2-cyclopentanediamine. Cage **5**-*R* is substantially larger than modules **1**, **3** and **4**. For example, the tetrahedron inscribed by the centres of the triangular faces of **5**-*R* has a volume that is 3.8 times larger than the comparable tetrahedron for cage **1** (Fig. S24). In this case, lattice energy calculations suggest homochiral window-to-window packing as the clear global energy minimum and this predicted structure is observed experimentally for **5**-*R* (Fig. 3d); again, DFT calculations agree broadly with the CSP calculated energy differences. To our knowledge, **5**-*R* (1704 g mol^{-1}) is the largest organic molecule to be successfully tackled by crystal structure prediction[16]. Numerous experiments involving crystallisation from mixtures of the modules **5**-*R* and **5**-*S* all led exclusively to homochiral crystals, in agreement with the predicted lattice energy preference over all hypothetical racemic structures. The crystalline solid **5**-*R* has larger pores (*c.f.*, Fig. 1b,c and Fig. 1d) and a greater pore volume (0.63 $cm^3 g^{-1}$) than any of the materials produced from the smaller cages **1**, **3** and **4**. The surface area for **5**-*R* (SA_{BET} = 1333 $m^2 g^{-1}$) exceeds all but one[15] of the porous molecular (non-network) crystals reported to date[9-14,24], and is comparable with the first generation of covalent organic frameworks[6]. This larger cage shows that it is possible to prepare molecular organic crystals with bespoke pore sizes, analogous with the well-known series of isoreticular MOFs[3] where pore size is defined by organic strut length. A future challenge will be to generalize this non-covalent assembly methodology. Non-identical

molecules do not, as a general rule, cocrystallize, and it may be necessary to incorporate specific complementary functionality in order to induce cocrystallization of dissimilar modules.

We have shown that porous cages can assemble in a modular fashion and, moreover, that the mode of assembly can be predicted accurately using lattice energy calculations. These particular structures are amenable to computation because the directional interlocking of neighbouring cages leads to large energy differences between hypothetical structures. By contrast, most other organic molecules give rise to many distinct possible crystal structures within a few kJ mol^{-1}.[16-17] Larger, conformationally flexible cage modules would be more challenging for these prediction methods, but significant recent advances have been made to deal with molecular flexibility[29-30]. Thus, the work presented here opens the way for *in silico* prediction of structure and properties for new candidate porous materials based solely upon 2-dimensional chemical sketches, thus allowing 'design by computational selection'.

The solution processability of the cage modules also means that the assembly approach can be extended to achieve structural control beyond the molecular length scale. For example, the (**3**-*S*, **3**-*R*) racemate is at least ten times less soluble than the homochiral modules, **3**-*S* and **3**-*R*, and this leads to spontaneous precipitation upon mixing of solutions of the two enantiomers (see video, Fig. S27). Well-defined porous (**3**-*S*, **3**-*R*) nanocrystals are formed (Fig. 4), thereby translating intermolecular heterochiral tecton interactions into nanoscale morphology control. Porous nanocrystals might enable particular applications for these solids in the future – for example, in chiral catalysis or separations.

METHODS SUMMARY

Synthesis of compounds. Cage **1**, cage **4**-*R*, and cage **3**-*R* were synthesized via a [4 + 6] cycloimination reaction involving triformylbenzene and the diamines ethylenediamine, (1*S*, 2*S*)-cyclopentanediamine, and (1*R*, 2*R*)-cyclohexanediamine, respectively, using an improved, higher-yielding synthetic procedure to that reported previously[12] (see Supporting Information). Cage **5**-*R* was synthesized by the [4 + 6] cycloimination reaction between tri(4-formylphenyl)amine and (*R*,*R*)-1,2-cyclopentanediamine. Cocrystals were grown from equimolar solutions of the partner cage modules. Details of the crystallographic analysis, crystal data, and gas sorption analysis are described in the Supplementary Information.

Crystal structure prediction. Crystal structures were generated in the most commonly observed space groups using a Monte Carlo simulated annealing search method. The lowest energy structures from the Monte Carlo search were then lattice energy minimised using anisotropic atom-atom potentials within the crystal structure modelling software DMACRYS[28]. Molecular geometries, generated by DFT single molecule optimisation, were treated as rigid throughout the predictions. Further details are given in the Supplementary Information.

DFT calculations. Cage pairs and crystal structures have been fully optimised in the mixed Gaussian and planewave code CP2K, using the TZVP-MOLOPT basis set in combination with GTH-pseudopotentials and a plane wave cutoff of 400Ry. Molecular and solid state calculations employed the BLYP and PBE functionals, respectively, both with Grimme-D3 dispersion correction.

References

1 Kondo, M., Yoshitomi, T., Seki, K., Matsuzaka, H. & Kitagawa, S. Three-dimensional framework with channeling cavities for small molecules: $\{M_2(4,4'\text{-bpy})_3(NO_3)_4 \cdot xH_2O\}_n$ (M = Co, Ni, Zn). *Angew. Chem., Int. Edit.* **36**, 1725-1727 (1997).

2 Li, H., Eddaoudi, M., O'Keeffe, M. & Yaghi, O. M. Design and synthesis of an exceptionally stable and highly porous metal-organic framework. *Nature* **402**, 276-279 (1999).

3 Eddaoudi, M. *et al.* Systematic design of pore size and functionality in isoreticular MOFs and their application in methane storage. *Science* **295**, 469-472 (2002).

4 Zhao, X. B. *et al.* Hysteretic adsorption and desorption of hydrogen by nanoporous metal-organic frameworks. *Science* **306**, 1012-1015, (2004).

5 Férey, G. *et al.* A chromium terephthalate-based solid with unusually large pore volumes and surface area. *Science* **309**, 2040-2042 (2005).

6 Côté, A. P. *et al.* Porous, crystalline, covalent organic frameworks. *Science* **310**, 1166-1170 (2005).

7 Deng, H. X. *et al.* Multiple functional groups of varying ratios in metal-organic frameworks. *Science* **327**, 846-850, (2010).

8 Nureki, O. *et al.* Enzyme structure with two catalytic sites for double-sieve selection of substrate. *Science* **280**, 578-582 (1998).

9 Barbour, L. J. Crystal porosity and the burden of proof. *Chem. Commun.*, 1163-1168 (2006).

10 Atwood, J. L., Barbour, L. J. & Jerga, A. Storage of methane and freon by interstitial van der Waals confinement. *Science* **296**, 2367-2369 (2002).

11 Tranchemontagne, D. J. L., Ni, Z., O'Keeffe, M. & Yaghi, O. M. Reticular chemistry of metal-organic polyhedra. *Angew. Chem., Int. Edit.* **47**, 5136-5147, (2008).

12 Tozawa, T. *et al.* Porous organic cages. *Nat. Mater.* **8**, 973-978, (2009).

13 Bezzu, C. G., Helliwell, M., Warren, J. E., Allan, D. R. & McKeown, N. B. Heme-like coordination chemistry within nanoporous molecular crystals. *Science* **327**, 1627-1630, (2010).

14 Jones, J. T. A. *et al.* On–off porosity switching in a molecular organic solid. *Angew. Chem., Int. Edit.*, 749-753, (2011).

15 Mastalerz, M., Schneider, M. W., Oppel, I. M. & Presly, O. A salicylbisimine cage compound with high surface area and selective CO_2/CH_4 adsorption. *Angew. Chem., Int. Edit.* **50**, 1046-1055 (2011).

16 Day, G. M. *et al.* Significant progress in predicting the crystal structures of small organic molecules – a report on the fourth blind test. *Acta Crystallogr. Sect. B-Struct. Sci.* **65**, 107-125, (2009).

17 Price, S. L. Computed crystal energy landscapes for understanding and predicting organic crystal structures and polymorphism. *Accounts Chem. Res.* **42**, 117-126, (2009).

18 Jansen, M., Doll, K. & Schön, J. C. Addressing chemical diversity by employing the energy landscape concept. *Acta Crystallogr. Sect. A* **66**, 518-534, (2010).

19 Ingleson, M. J., Barrio, J. P., Guilbaud, J. B., Khimyak, Y. Z. & Rosseinsky, M. J. Framework functionalisation triggers metal complex binding. *Chem. Commun.*, 2680-2682, (2008).

20 Desiraju, G. R. Supramolecular synthons in crystal engineering – a new organic-synthesis. *Angew. Chem., Int. Edit.* **34**, 2311-2327 (1995).

21 Simard, M., Su, D. & Wuest, J. D. Use of hydrogen bonds to control molecular aggregation. Self-assembly of three-dimensional networks with large chambers. *J. Am. Chem. Soc.* **113**, 4696-4698 (1991).

22 Wuest, J. D. Engineering crystals by the strategy of molecular tectonics. *Chem. Commun.*, 5830-5837 (2005).

23 Hof, F., Craig, S. L., Nuckolls, C. & Rebek, J. Molecular encapsulation. *Angew. Chem., Int. Edit.* **41**, 1488-1508 (2002).

24 McKeown, N. B. Nanoporous molecular crystals. *J. Mater. Chem.* **20**, 10588-10587 (2010).

25 Wheeler, K. A., Grove, R. C., Davis, R. E. & Kassel, W. S. Quasiracemic materials – Rediscovering Pasteur's quasiracemates. *Angew. Chem., Int. Edit.* **47**, 78-81, (2008).

26 Dance, I. & Scudder, M. Supramolecular motifs: sextuple aryl embraces in crystalline M(2,2'-bipy)$_3$ and related complexes. *J. Chem. Soc., Dalton Trans.*, 1341-1350 (1998).

27 Day, G. M., Motherwell, W. D. S. & Jones, W. Beyond the isotropic atom model in crystal structure prediction of rigid molecules: Atomic multipoles versus point charges. *Cryst. Growth Des.* **5**, 1023-1033, (2005).

28 Price, S. L. *et al.* Modelling organic crystal structures using distributed multipole and polarizability-based model intermolecular potentials. *Phys. Chem. Chem. Phys.* **12**, 8478-8490, (2010).

29 Karamertzanis, P. G. & Pantelides, C. C. Ab initio crystal structure prediction. II. Flexible molecules. *Mol. Phys.* **105**, 273-291, (2007).

30 Görbitz, C. H., Dalhus, B. & Day, G. M. Pseudoracemic amino acid complexes: blind predictions for flexible two-component crystals. *Phys. Chem. Chem. Phys.* **12**, 8466-8477, (2010).

Acknowledgements. We thank EPSRC (EP/H000925/1) and the Dutch Polymer Institute for funding. AIC is a Royal Society Wolfson Merit Award holder; AT is a Royal Society University Research Fellow.

Acknowledgements. We thank EPSRC (EP/H000925/1), the Dutch Polymer Institute, and the University of Liverpool for funding. AIC is a Royal Society Wolfson Merit Award holder; AT is a Royal Society University Research Fellow. We thank Mr Rob Clowes for gas sorption analysis and Dr S Higgins for assistance with robotic liquid handlers.

Author Contributions. JTAJ prepared (**1**-*S*, **3**-*R*), contributed to PXRD analysis, carried out high-throughput cocrystallization screening experiments, and generally coordinated the experimental work; TH prepared (**3**-*S*, **3**-*R*), (**4**-*S*, **3**-*R*), the nanocrystals thereof, and carried out microscopy; JTAJ and TH did the gas sorption analysis; XW synthesized module **5**; DJA contributed to the cage synthesis; JB, MS, SYC and AS performed the crystallography; KEJ, AT, FC, and BS performed molecular simulations, in particular the DFT studies; GMD led the crystal structure prediction; AIC designed the project and wrote the paper with contributions from all co-authors.

Correspondence and requests for materials should be addressed to AIC

Figure 1 Modular assembly of porous organic cages. a, Structures of four organic cage modules (hydrogens omitted for clarity). Cage **1** is shown as the *S* enantiomer but this module is amphichiral and can interconvert between *R* and *S* forms. **b,** Crystal structures for porous organic solids formed from these modules, Connolly surface shown in yellow (probe radius = 1.82 Å). From left to right: quasiracemic cocrystal (**1**-*S*, **3**-*R*), racemic crystal (**3**-*S*, **3**-*R*), and chiral crystal **5**-*R*.

Figure 2 Window-to-window assembly results in porosity. a, Helical chirality in **1** is dynamically resolved by heterochiral cocrystallization with **3-*R***. The schematic packing diagram for (**1**-*S*, **3**-*R*) shows the centres of modules **1**-*S* and **3**-*R* as green and red spheres, respectively; orange spheres represent interstitial voids that are not connected to the diamondoid pore network, illustrated in yellow. **b,** Nitrogen gas sorption analysis for crystals and cocrystals shows that pore volume and pore size can be varied systematically, as in isoreticular networks. **c,** Scheme showing packing for various crystals and cocrystals.

Figure 3 Three dimensional cage assembly can be predicted computationally. Lattice energy rankings rationalize the heterochiral packing preference for the (**1**, **3**) cocrystal (structure **a** favoured over all hypothetical homochiral predicted structures), the racemic packing preference for cage **3** (structure **c** favoured over **b**), and the chiral preference for **5** (**d** favoured over all hypothetical racemates). Packing diagrams **a**–**d** show the excellent fit between the calculated global minimum structures (blue) and the experimentally-determined structures (red). The predicted (**1**-*S*, **3**-*R*) structure in **a** is slightly less symmetrical than the observed *R*3 space group symmetry and the *P*1 unit cell is shown.

Figure 4 Module assembly in solution can be used to produce porous nanoparticles. Mixing solutions of **3**-*S* and **3**-*R* leads to rapid precipitation of racemic octahedral nanocrystals of (**3**-*S*, **3**-*R*) with an average diameter of 130 nm (SA_{BET} = 873 $m^2\ g^{-1}$).

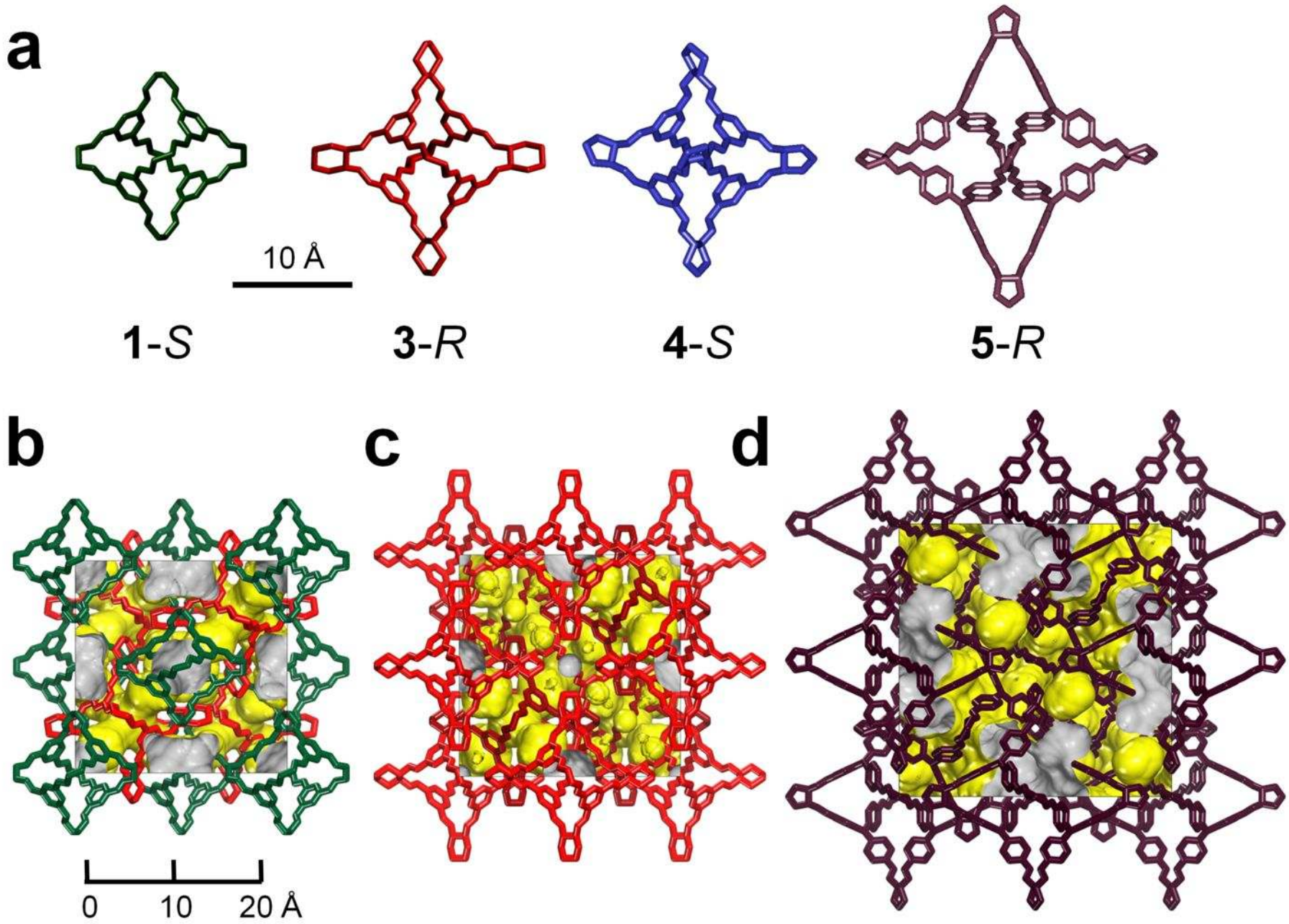
a
10 Å
1-S
3-R
4-S
5-R
b
c
d
0
10
20 Å

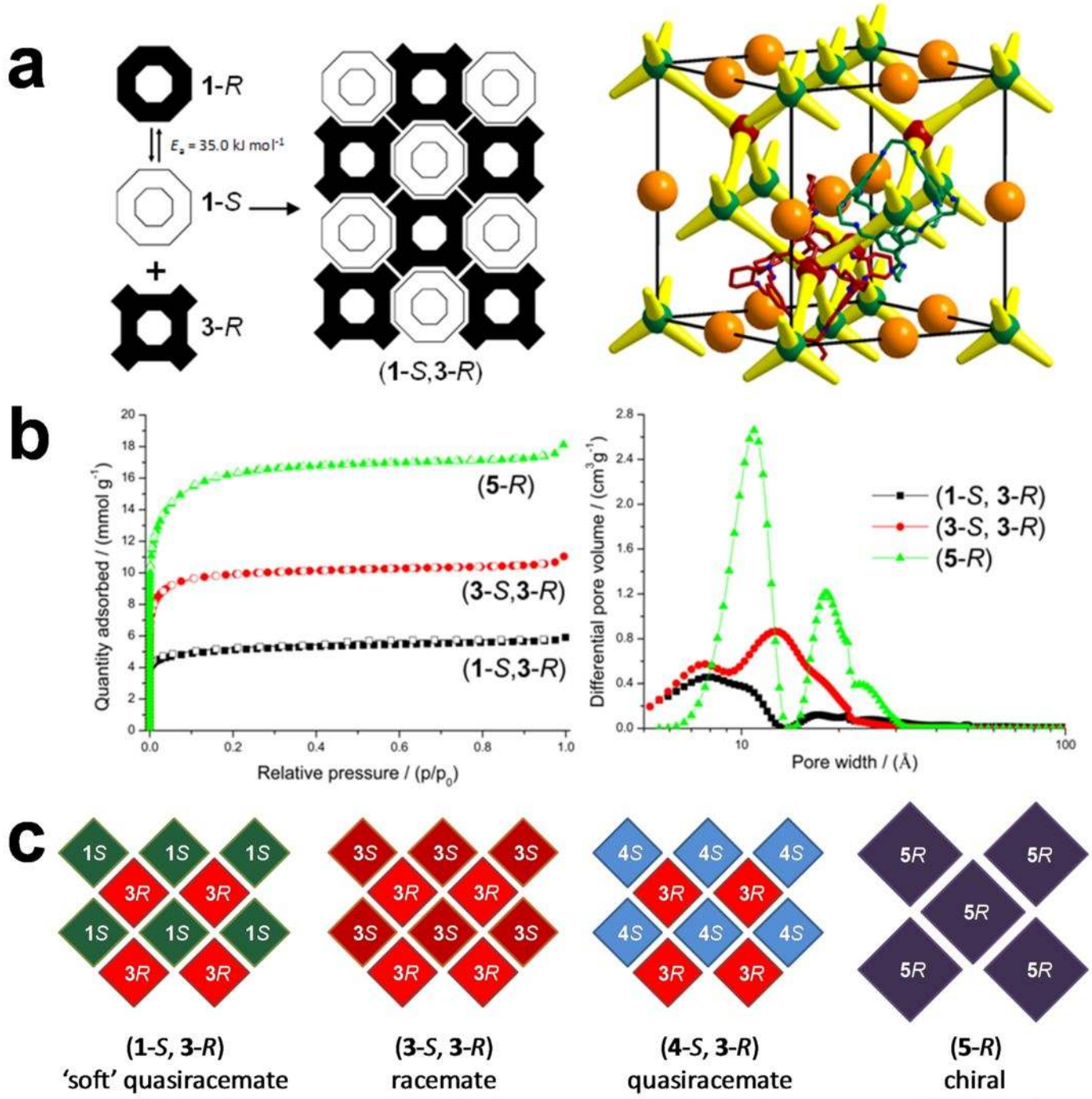
a
1-R
E_a = 35.0 kJ mol^{-1}
1-S
+
3-R
(1-S,3-R)
b
(5-R)
(3-S,3-R)
(1-S,3-R)
Quantity adsorbed / (mmol g^{-1})
Relative pressure / (p/p$_0$)
Differential pore volume / (cm^{3}g^{-1})
Pore width / (Å)
(1-S, 3-R)
(3-S, 3-R)
(5-R)
c
1S
3R
3S
4S
5R
(1-S, 3-R)
'soft' quasiracemate
437 m^2 g^{-1}
(3-S, 3-R)
racemate
873 m^2 g^{-1}
(4-S, 3-R)
quasiracemate
980 m^2 g^{-1}
(5-R)
chiral
1333 m^2 g^{-1}

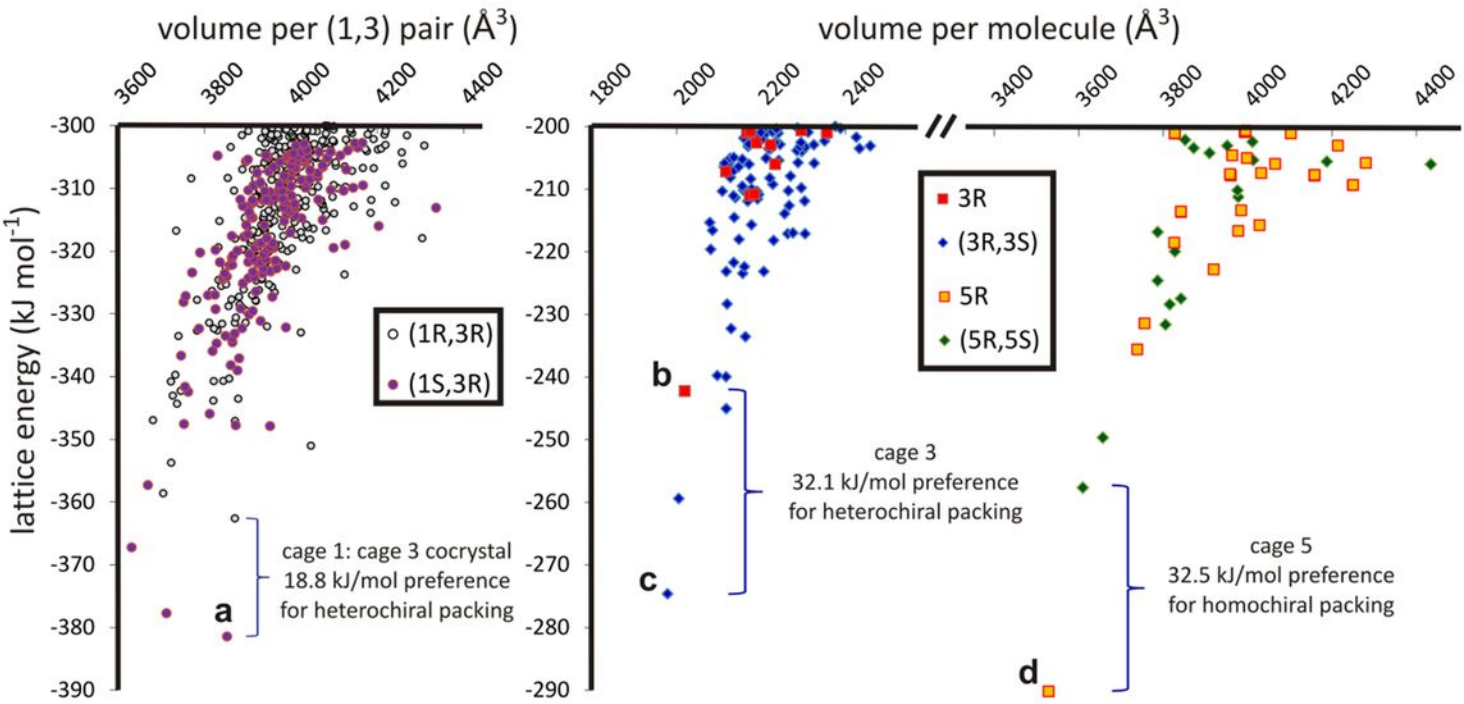
volume per (1,3) pair (Å^3)
volume per molecule (Å^3)
lattice energy (kJ mol^{-1})
(1R,3R)
(1S,3R)
3R
(3R,3S)
5R
(5R,5S)
a
b
c
d
cage 1: cage 3 cocrystal
18.8 kJ/mol preference
for heterochiral packing
cage 3
32.1 kJ/mol preference
for heterochiral packing
cage 5
32.5 kJ/mol preference
for homochiral packing

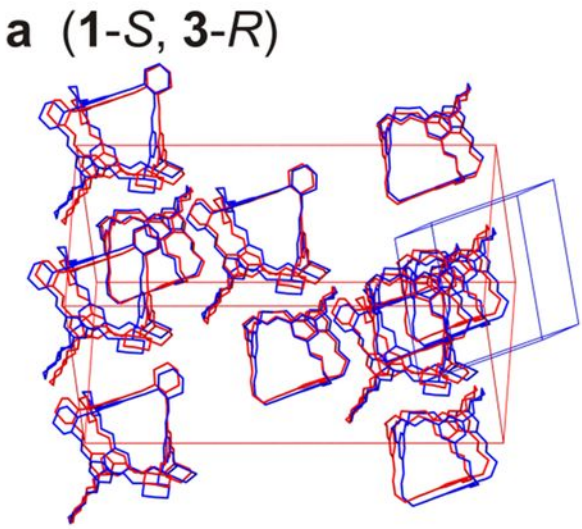
a (1-S, 3-R)

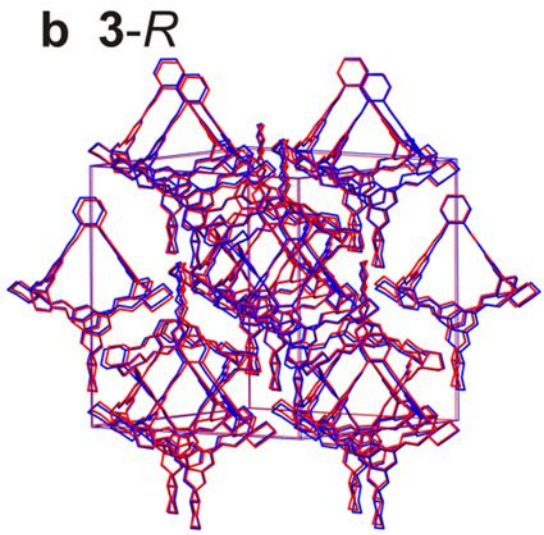
b 3-R

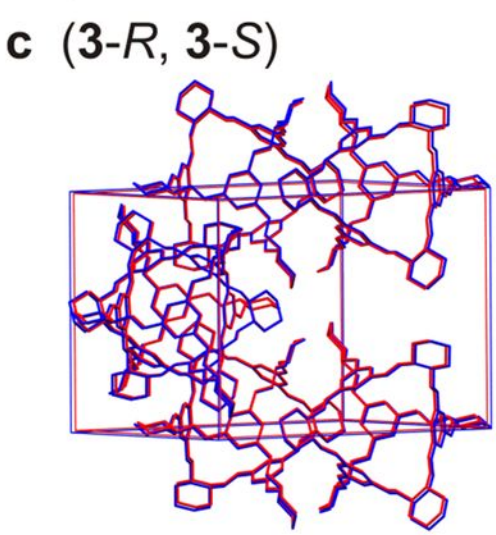
c (3-R, 3-S)

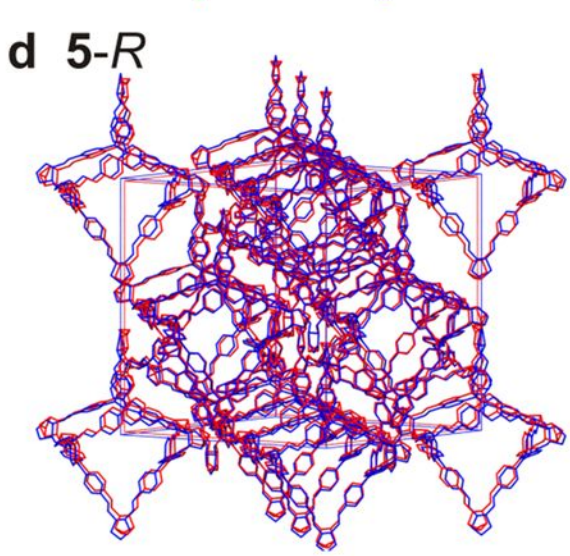
d 5-R

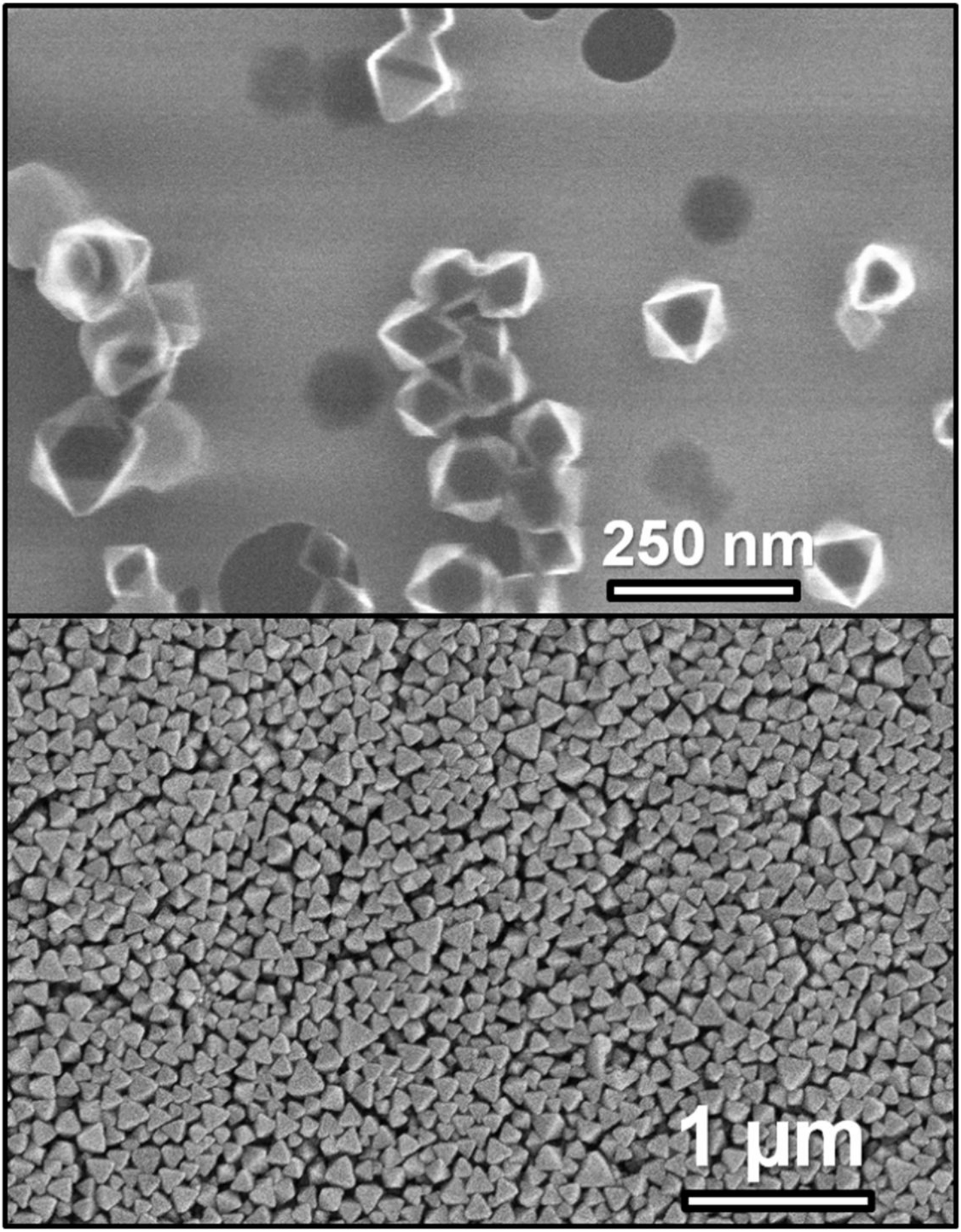
250 nm
1 µm